Construction and Building Materials 353 (2022) 129097

Contents lists available at ScienceDirect

Construction and Building Materials

journal homepage: www.elsevier.com/locate/conbuildmat

Effect of recycled concrete aggregate features on adhesion properties of asphalt mortar-aggregate interface

Haisheng Ren [a,d], Zhendong Qian [a,*], Bin Lin [c], Qibo Huang [a,b], Maurizio Crispino [d], Misagh Ketabdari [d]

[a] Intelligent Transportation System Research Center, Southeast University, Nanjing 211189, China
[b] Foochow Transportation Department, Fuzhou 350004, China
[c] CCCC Second Highway Consultants Co., Ltd., Wuhan 430118, China
[d] Department of Civil and Environmental Engineering, Politecnico di Milano, Milan 20133, Italy

ARTICLE INFO

Keywords:
RCA feature
Asphalt-RCA interface
Cohesive zone model
GA-BP artificial neural network model
Interface adhesions behavior

ABSTRACT

Asphalt-aggregate interface's adhesion properties commonly affect the damage initiation and evolution within asphalt concrete materials, related to pavement durability and quality. The scope of this research was to investigate the influence of Recycled Concrete Aggregate (RCA) features on asphalt mortar-aggregate interface adhesion. Firstly, a three-dimensional reconstruction model of RCA was carried out using X-ray CT tomography and digital image processing. In this regard, five feature indicators, namely cement mortar content, sphericity, flat and elongated ratio, angularity, and surface texture, were proposed. Based on a bilinear cohesive zone model, the interface damage behavior of asphalt mortar-RCA was investigated by using a uniaxial compression simulation. Finally, a GA-BP artificial neural network was conducted to predict and quantify the effect of each feature indicator of RCA on interface adhesion. The results showed that when RCA had lower cement mortar content, higher sphericity value, and smoother surface, the asphalt mortar-RCA system was less prone to interface adhesion failure. The 5-14-1 GA-BP artificial neural network proposed in this study showed very good performance in predicting the interfacial dissipation damage energy with a mean-squared error value of 3.52×10^{-4} for testing dataset. The cement mortar content parameter exhibited a remarkable influence on the interface adhesion property, and its global contribution to the interfacial dissipation damage energy (0.3486) was more than twice that of the surface texture parameter (0.1316). In future studies, the performance characteristics of cement mortar can be further investigated, thereby proposing RCA's performance optimization technology.

1. Introduction

In recent decades, a series of environmental pollution problems caused by construction and demolition waste (C&DW) have attracted the attention of many countries [1,2]. On this noticeable issue, using waste concrete as recycled aggregate instead of natural aggregate to produce road material is considered as the most reasonable solution, which has become a hotspot research topic in the field of road engineering [3–5]. At present, the research on asphalt mixture containing recycled concrete aggregate (RCA) mainly focuses on three directions, including physicochemical properties of RCA, performance improvement approach of RCA, and performance evaluation of RCA asphalt mixture [6,7]. For example, Juan et al. [8] pointed out that RCA showed a linear growth in Los Angeles abrasion loss with the increase of cement mortar content remaining on RCA. The stripping aggregate phase primarily contained cement mortar powder. Lee et al. [9] evaluated the mechanical properties of the interface between cement mortar and original natural aggregate. Results indicated that the weak interaction at the interfacial transition zone and microcracks in cement mortar significantly degraded the mechanical strength of RCA. Thomas et al. [10] addressed that the crushing method of waste cement concrete resulted in high potential of fracture surface and angularity for RCA. Tam et al. [11] compared the improvement levels of RCA strength with various inorganic acid types, concentrations, and soaking times. Pasandín et al. [12] utilized boiling water and rolling bottle tests to reveal the influence of asphalt grade, mineral filler type, and RCA

* Corresponding author.
E-mail addresses: ren_hs510@seu.edu.cn (H. Ren), qianzd@seu.edu.cn (Z. Qian), huangqibo@seu.edu.cn (Q. Huang), maurizio.crispino@polimi.it (M. Crispino), misagh.ketabdari@polimi.it (M. Ketabdari).

https://doi.org/10.1016/j.conbuildmat.2022.129097
Received 17 February 2022; Received in revised form 5 September 2022; Accepted 6 September 2022
Available online 13 September 2022

pretreatment method on the affinity between asphalt and RCA, and the relevant improvement approach was suggested. Nejad et al. [13] analyzed the fatigue characteristics of RCA asphalt mixture through using an indirect tensile fatigue test. The results expressed that the asphalt mixture with 100 % RCA fine aggregate still showed excellent fatigue resistance.

Many research results show that asphalt mixture's internal damage initiation and evolution mainly begins at the asphalt-aggregate interface [14,15]. And the Interface Transition Zone (ITZ) between asphalt and aggregate plays a significant role in determining the comprehensive performance of asphalt mixture [16,17]. Mo et al. proposed a new set-up consisting of Dynamic Mechanical Analyzer and Dynamic Shear Rheometer to measure the development of asphalt-stone adhesion damage, and their corresponding finite element modelling tests were performed to obtain the better proper interpretation. The results indicated that stone morphology had an important influence on the performance of ITZ [37]. Lu et al. used the nano-mechanics method to build the asphalt-aggregate interface modelling and explore the molecular origin of interfacial deformation and failure processes under tensile or confined shear loading [38]. Wang et al. proposed an atomistic simulation of moisture-induced damage behavior at asphalt-aggregate interface based on the molecular dynamic method. The results illustrated that increasing temperature and moisture content on the interface reduced its adhesion strength, and asphalt binder's chemical compositions showed a dramatic influence on the adhesion quality of asphalt-aggregate interface [39]. Kuang et al. reported that limestone showed a more complicated surface texture compared to granite, resulting in a better adhesion property between asphalt and limestone particles [40]. Horgnies et al. performed Environmental Scanning Electronic Microscope and Energy Dispersive X-ray (EDX) spectrometry to analyze the chemical composition of asphalt-aggregate interface, and built the relationship between interfacial composition and adhesion property [41].

Despite numerous researches having addressed the property characteristics of RCA and corresponding asphalt mixture, some efforts have attempted to evaluate the mechanical behavior and microstructure features of ITZ in RCA asphalt mixture. Hu et al. compared the ITZ of asphalt-nature aggregate and asphalt-RCA through scanning electron microscopy and X-ray computed tomography images, and evaluated the fracture resistance and interface mechanical behavior of RCA asphalt mixture by using semi-circle bending test [42]. Huang et al. conducted nanoindentation test, backscattered electron image-analysis, and energy dispersive spectroscopy to investigate the thickness, microstructure, and mechanical characteristics of ITZ in RCA asphalt mixture. The results indicated that the region in ITZ closer to cement mortar and brick showed a lower elastic modulus and hardness. They presented that the interface adhesion properties and the relationship of ITZ's micro-mechanical and RCA asphalt mixture's macro-mechanical behavior could be further evaluated [17].

Based on previous research results, this study focuses on the ITZ adhesion behavior of asphalt mixture containing different RCA particles, because the aggregate features (e.g., shape, angularity) also play a critical role in influencing the interface adhesion quality, especially for the RCA. The primary objectives of this study are concerned with three areas: (1) to analyze the adhesion damage initiation and evolution at asphalt mortar-RCA interface through numerical simulation test; (2) to predict the adhesion failure characteristics of different asphalt mortar-RCA interfaces using an artificial neural network model; (3) to quantify the contribution of each RCA feature parameter to interface adhesion quality.

2. Quantification of RCA features

2.1. 3D reconstruction model of RCAs

In this study, the RCA source was provided by the aggregate plant through crushing the construction and demolition waste, and its physical properties are listed in Table 1. RCA particles ranged in size from 2.36 mm to 26.5 mm.

As a non-destructive imaging technology, X-ray Computed Tomography (X-ray CT) scanning has been widely used by many civil engineers to evaluate the internal structural characteristics of civil engineering materials [18,19]. A total of 125 RCA particles placed in a cube container were scanned using X-ray CT with a scanning interval of 0.1 mm. Then, the CT images of RCA were subjected to grayscale transformation, median filtering, and binarization by Digital Image Processing (DIP) analysis to obtain their morphology parameters. The saved CT images were Red Green Blue (RGB) images with 24 bits size of each pixel, and they were converted to relevant Gray Scale images (8 bits per pixel size) by using weighted average method. The gray values changing from 0 to 255 represented the brightness of the image ranging from fully black to fully white. Within the RCA particle, cement mortar remaining, original aggregate and air voids showed different gray levels in accordance with their material density. Median filtering technique was utilized to reduce the isolated noise in RCA gray images, which helped to improve the image segmentation quality. The maximum classes square error method (Otsu) was carried out to determine an ideal threshold value for binarization, and the RCA gray image could be divided into two parts, namely areas of interest (AOI) and background. As a result, the AOIs consisting of cement mortar remaining, original aggregate and air voids phases were extracted and identified. And the bonding status between original aggregate particles of RCA was further eliminated through distance-map and watershed segmentation method. After image processing, the extracted RCA microstructure information was finally imported into Avizo software. And the 3D models of different RCAs were reconstructed, as shown in Fig. 1.

2.2. Indicator selection for RCA features

In the RCA asphalt mixture system, the properties of cement mortar remaining and original aggregate of RCA both have impacts on the adhesion quality of the asphalt-aggregate interface [20]. Therefore, we proposed four parameters to quantify RCAs' features in this study. Avizo software was adopted to extract the morphology data of reconstructed 3D RCA particles, thereby, the values of RCA feature parameters were calculated.

2.2.1. Cement mortar content

The mechanical behavior of cement mortar adsorbed on aggregate surface is different from that of natural aggregate. Using Cement Mortar Content (CMC) in RCA as an indicator to evaluate the effect of cement mortar on asphalt mortar-RCA interface adhesion, as shown in Eq. (1).

$$CMC = \frac{V_C}{V_{RA}} \times 100\% \quad (1)$$

where V_C and V_{RA} are the volumes of cement mortar attached to the reconstructed 3D RCA particles and the total volume of aggregate, respectively, mm^3.

2.2.2. Shape

The shape characteristics represent the contour of aggregate boundary, and 3D Sphericity (S_{3D}) is a common indicator to quantify the

Table 1
Physical properties of RCA and natural aggregate.

Physical properties	RCA	Natural aggregate
Bulk density, g/cm3	2.66	2.75
Water absorption, %	5.04	0.65
Crush value, %	24.18	15.98
Abrasion value, %	25.25	8.99
Flakiness	12.40	8.50

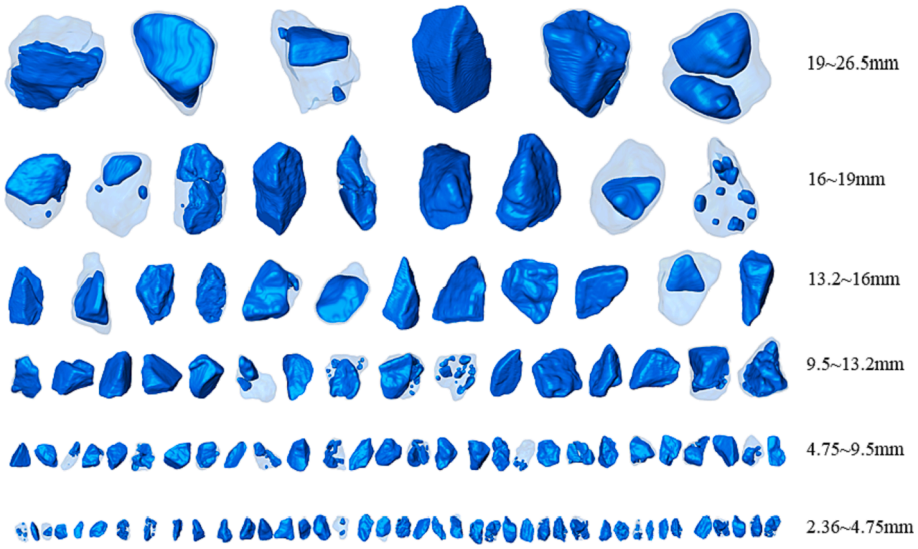

Fig. 1. 3D reconstruction models of RCAs.

degree of similarity between the shape of aggregate particles and a sphere, with values ranging from 0 to 1. The S_{3D} value closer to 1 indicates that aggregate looks more like a spherical particle. The S_{3D} value of a cube-shaped aggregate is approximately 0.81. The S_{3D} parameter of aggregate can be calculated by Eq. (2).

$$S_{3D} = \frac{\pi}{A_{3D}}\left(\sqrt{3}\frac{6V_{3D}}{\pi}\right)^2 \tag{2}$$

where A_{3D} = surface area of aggregate particles, mm^2; V_{3D} = volume of aggregate particles, mm^3.

The Flat and Elongated (FE) ratio refers to the ratio of the maximum axial length of coarse aggregate particle to its minimum axial length. Asphalt concrete contains aggregate with high FE ratios, which easily leads to the increase of air void and the potential of native defects in internal structure [21]. The following equation can be used to calculate the FE_{3D} ratio of RCA particles.

$$FE_{3D} = \frac{L_{max}}{w_{min}} \tag{3}$$

where, w_{min} represents the minimum Feret diameter of aggregate particles, mm; L_{max} describes the maximum Feret diameter of aggregate particles in the direction orthogonal to w_{min}, mm.

2.2.3. Angularity

Existing research shows [22] that using the aggregates with high sphericity, low FE ratio, and outstanding angularity is beneficial to prepare high-performance asphalt concrete (e.g., excellent mechanical strength and deformation resistance). Therefore, the 3D Angularity Index (AI_{3D}) calculated by Eq. (4) was also determined as a parameter of RCA features.

$$AI_{3D} = \frac{A_{3D}}{A_{ellipsoid}} \tag{4}$$

where, A_{3D} = surface area of RCA particle, mm^2; $A_{ellipsoid}$ = surface area of equivalent ellipsoid of RCA, mm^2.

2.2.4. Surface texture

The aggregate with complicated surface texture plays a significant role in improving the skid resistance and mechanical strength of asphalt pavement. Based on mathematical morphology, the 3D Surface Texture (ST_{3D}) of RCA particle was calculated by using opening operations, as shown in Eq. (5) [23].

$$ST_{3D} = \frac{V_{3D} - V_{open}}{V_{3D}} \times 100\backslash\% \tag{5}$$

where, V_{3D} and V_{open} are the volumes of RCA particles before and after opening operations, respectively, in voxel.

3. Numerical simulation based on cohesive zone model

3.1. Cohesive zone model

A large number of researches have confirmed that the Cohesive Zone Model (CZM) based on a bilinear traction-separation law can precisely analyze the fracture behavior in asphalt mixture and the interface between asphalt mortar and coarse aggregate [24–26]. The constitutive law of bilinear CZM is used to build the relationship between surface traction and crack opening displacement, as shown in Fig. 2. In the bilinear law, three material parameters are required, namely, cohesive strength (T^o), separation (Δ), and cohesive fracture energy (G_f). The G_f calculated by Eq. (6) represents the area of the traction-separation curve.

$$G_f = \int_0^{\Delta^c} T(\Delta)d\Delta = \frac{1}{2}T^o\Delta^c \tag{6}$$

Bilinear CZM damage criterion contains the damage initiation and evolution. The damage initiation criterion is defined as a critical condition for the traction components to change from elastic phase to damage initiation phase [27]. In this study, the quadratic nominal stress criterion contained in ABAQUS software was designated as the damage initiation criterion in bilinear CZM, which is expressed by Eq. (7) and Eq. (8). Once the sum of the squares of all nominal stress (normal and tangential components shown in Fig. 2a and Fig. 2b) is equal to one, it indicates that the interface damage of asphalt-aggregate begins.

$$\left\{\frac{\langle T_n\rangle}{T_n^o}\right\}^2 + \left\{\frac{\langle T_s\rangle}{T_s^o}\right\}^2 = 1 \tag{7}$$

$$\langle T_n\rangle = \begin{cases} T_n, T_n \geqslant 0; for{\cdot}tension \\ 0, T_n < 0; for{\cdot}compression \end{cases} \tag{8}$$

where, T_n and T_s are nominal stresses in normal and tangential, respectively; the subscript o represents the maximum stress at the onset of damage initiation; Macaulay bracket operator $< >$ indicates that the normal compressive stress has no effect on the damage initiation.

During the damage evolution of asphalt-aggregate interface, the

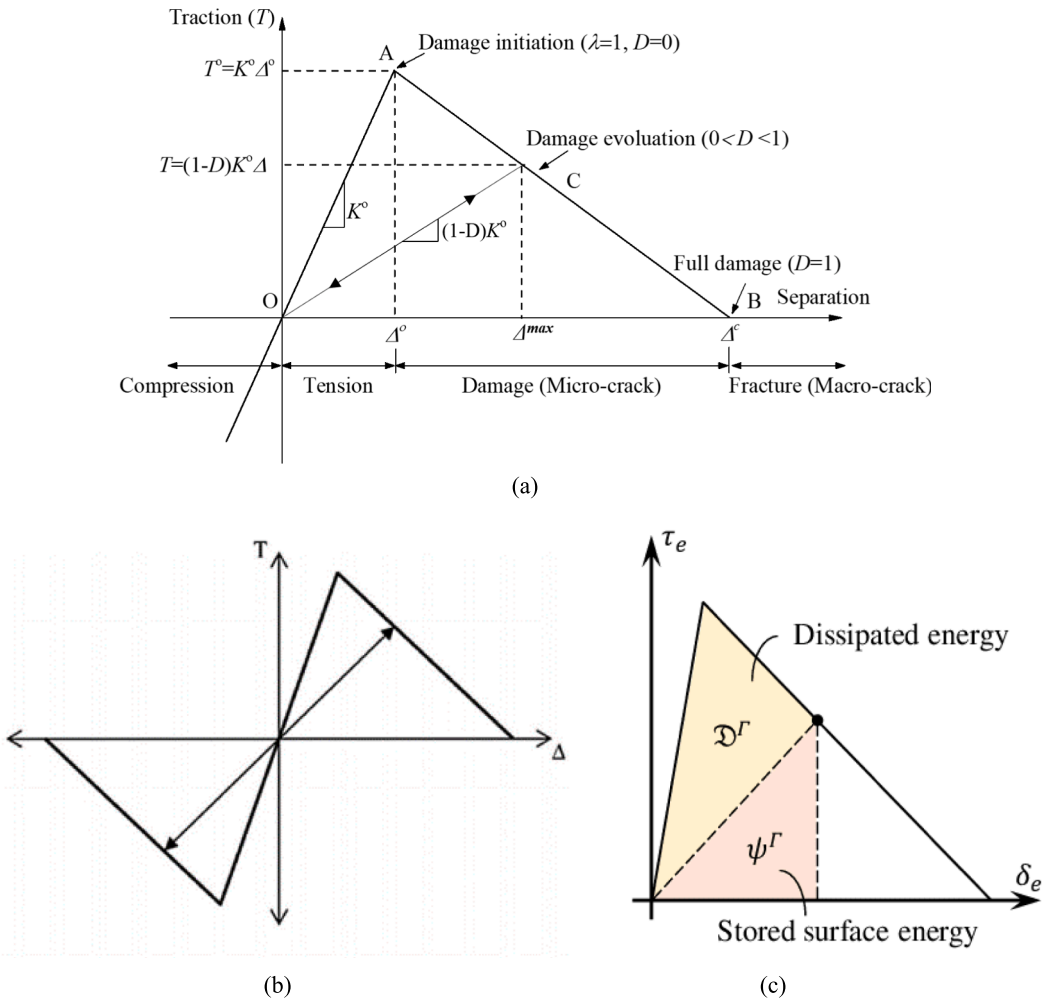

Fig. 2. Constitutive relationship of bilinear CZM; (a) normal; (b) tangential; (c) energy evolution.

cohesive stiffness degrades with crack opening displacement. A scalar stiffness degradation parameter (SDED) expressed in Eq. (9) was carried out to describe the damage evolution of asphalt mortar-RCA interface. The SDED value ranges between 0 and 1, where SDED = 0 illustrates non-damage on the interface, while SDED = 1 represents complete interface failure, and macro-cracks appear on the interface. In addition, the energy-based approach shows a better capacity to quantify the evolution stage of micro-crack initiation to macro-crack propagation. In this study, based on the fracture energy results of bilinear CZM, a Dissipation Damage Energy (DDE) indicator shown in Fig. 2(c) was also proposed to evaluate the damage evolution of asphalt-aggregate interface with loading time.

$$SDEG = \frac{\Delta^c(\Delta^{\max} - \Delta^o)}{\Delta^{\max}(\Delta^c - \Delta^o)} \tag{9}$$

where Δ^c is the effective separation at complete adhesion failure of interface; $\Delta^{\max}$ describes the maximum effective separation during loading; and Δ^o represents the effective separation at damage initiation state.

3.2. Model parameters

In order to successfully implement the numerical simulation test of asphalt mortar-RCA interface, it is necessary to obtain some material parameters through laboratory tests. At first, the cement mortar remaining and original aggregate contained in RCA were defined as linear elastic materials, and their Young's modulus was measured by nanoindentation test [43–44]. The asphalt mortar containing 50 % RCA (by weight of total mortar) was specified as a linear viscoelastic material, and its linear viscoelastic behavior at 60℃ was fitted by Generalized Maxwell model. The relevant parameters of the model were converted into Prony series and input into ABAQUS software. Additionally, the CZM parameters, (e.g., interface adhesion strength, fracture energy and initiation stiffness) were obtained by the three-point bending beam test [33] and interlayer shear strength test [34]. The results are shown in Table 2.

Table 2
CZM parameters of asphalt mortar-RCA interface at 60℃.

Interface type	Young's modulus/ GPa	Initiation stiffness K^o/ GPa	Adhesion strength T^o/ MPa	Fracture energy G_f/ N·m^{-1}	f
Asphalt mortar-cement mortar	—	8.0	1.2	40	0.5
Asphalt mortar-original aggregate	—	30	1.5	50	0.5
Cement mortar	20	—	—	—	—
Original aggregate	65	—	—	—	—

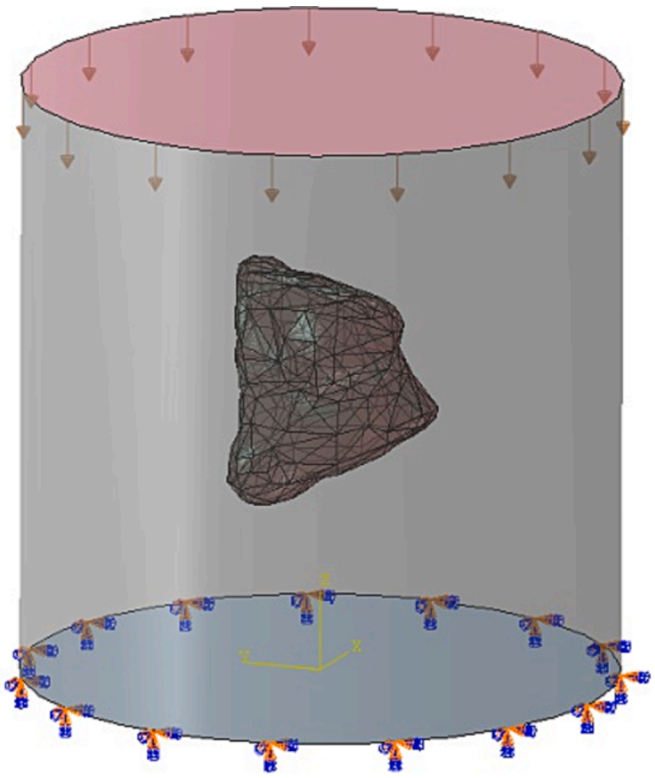

Fig. 3. Uniaxial compression simulation using ABAQUS software.

3.3. Uniaxial compression simulation

Finite Element Method (FEM) has been adopted by many researchers for its excellent ability in characterizing the internal microstructure failure of materials. In this study, ABAQUS finite element software was carried out to simulate the uniaxial compression test and evaluate the damage evolution of the asphalt mortar-RCA interface [16]. First, the STL files of reconstructed 3D RCA particles and cement mortar remaining obtained from Avizo software were input to ABAQUS software. The cement mortar adsorbed on the surface of RCA was subtracted from the RCA by using Boolean calculation to obtain the original aggregate part. The interface of the original aggregate and imported cement mortar parts were rebounded, and a new RCA was assembled in the software. A cylindrical specimen model of asphalt mortar with a diameter of 50 mm and a height of 50 mm was then built, and the new RCA particle was moved inside the specimen to ensure its center of gravity coincide. Through the same operation (i.e., Boolean calculation), a cavity specimen was obtained and re-assembled with RCA particle to generate the simulated specimen of asphalt mortar containing RCA, as listed in Fig. 3. During the numerical simulation process of the uniaxial compression test, the top surface of the cylindrical specimen was uniformly loaded with a displacement rate of 0.02 mm/s, and the loading time was designated as 100 s, while the bottom surface of the cylindrical specimen was fixed. At last, the CZM was carried out with corresponding model parameters to measure the mechanical behavior of the asphalt mortar-RCA interface under load, including the results of DDE and SDEG parameters.

4. GA-Based BP artificial neural network

4.1. Preparation of prediction model

It is worth noting that in the numerical simulation, DDE and SDEG indicators were adopted to quantify the total effect of five RCA parameters on the interface adhesion. Therefore, each parameter's influence was evaluated by using the Back-Propagation Artificial Neural Network optimized by a Genetic Algorithm (GA-based BP-ANN). With excellent robustness and fault tolerance, the ANN model is gradually playing an important role in the complex nonlinear analysis. The genetic algorithm shows the ability to iteratively search for the best initial weights and thresholds of BP-ANN, thereby obtaining more accurate prediction results. The feasibility of the GA-based BP-ANN model has been verified by many researchers [28,29]. Based on the numerical simulation results, five RCA parameters, namely CMC, S_{3D}, FE_{3D}, AI_{3D}, and ST_{3D}, were designated as input neurons, while DDE was set as output neuron. A three-layer neural network model was built in the commercial MATLAB software, as shown in Fig. 4.

In the GA-based BP-ANN model, the parameter data of 125 RCAs and corresponding DDE results after loading for 100 s were prepared as the database. The database was randomly divided into three groups, including 95 training samples, 15 validation samples and 15 test samples. All data were normalized to eliminate the influence of the magnitude difference between input and output data on the prediction accuracy of the network model, as outlined in Eq. (10) and Eq. (11).

$$X = \frac{x - x_{min}}{x_{max} - x_{min}} \times (b - a) + a \tag{10}$$

$$x = \frac{X - a}{b - a} \times (x_{max} - x_{min}) + x_{min} \tag{11}$$

where X represents normalized output data; x is the original data; x_{max} and x_{min} are the maximum and minimum values in the original database, respectively; a and b respectively express the upper and lower limit of normalized data.

In the training of network model, the propagation functions of hidden layer and output layer were respectively defined as Sigmoid function and pure linear function (i.e. $\varphi(x) = 1/(1 + e^{-x})$ and $\psi(x) = x$). As a result, when the data x_i was input in the network model, the predicted data O_s output by the model was expressed by Eq. (12). Moreover, Mean-Squared Error (MSE) was computed to evaluate the effective performance of the prediction model, which was required to be less than 0.001. It can be calculated by Eq. (13).

$$O_s = \psi\left[\sum w_{j1}\varphi\left(\sum (w_{ij}x_i + b_j) + b_k\right)\right] \tag{12}$$

$$MSE = \frac{\sum_{i=1}^{S}(T_i - O_i)^2}{S} \tag{13}$$

where S = total number of model samples; T = numerical simulation output (i.e. normalized DDE); O = predicted output of the network model; w = connection weight of the network model; b = input threshold of the network model.

4.2. Sensitivity analysis of influence factors

A large number of sensitivity analysis methods (e.g., PaD method, Perturb method and Profile method) have been proposed to evaluate the effect of input factors on output results [30,31]. However, most methods focus on ranking the influencing factors. As a result, the influence of each input factor and the interconnection between them cannot be determined effectively. In the current study, a Comprehensive Sensitivity Analysis (CSA) approach was applied to expose the mentioned influence mechanisms between RCA features and interface adhesion in the network model. More details about the CAS approach can be found in the previous research conducted by the authors of this study [32]. After the training of network model, it was assumed that the asphalt mortar-aggregate interface's dissipation damage energy, $y = f(M)$, can be differentiated at the input sample point, M (x_1, x_2, x_3, x_4, x_5). Therefore, its derivative at the M point was calculated by Eq. (14). The predicted output calculated by Eq. (12) was input into Eq. (14) to obtain the local relative contribution (d_{ik}) of the variable (x_i) and the global relative contribution of each input factor to the interfacial dissipation

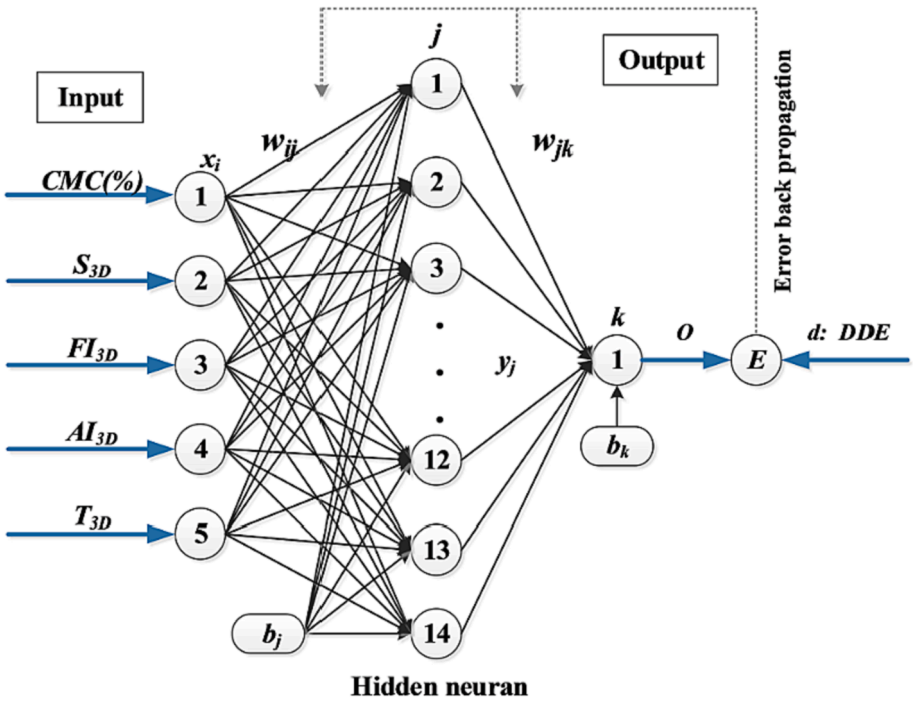

Fig. 4. Logical structure designed for the three-layer ANN model.

damage energy. Then, the Root Mean Square (RMS) was proposed to compare the global relative contribution between each input factor, as shown in Eq. (16).

$$\mathrm{d}y = \mathrm{grad}\, f(M)\cdot \mathrm{d}\vec{M} = \frac{\partial y}{\partial x_1}\mathrm{d}x_1 + \frac{\partial y}{\partial x_2}\mathrm{d}x_2 + \frac{\partial y}{\partial x_3}\mathrm{d}x_3 + \frac{\partial y}{\partial x_4}\mathrm{d}x_4 + \frac{\partial y}{\partial x_5}\mathrm{d}x_5 \quad (14)$$

$$d_{ik} = \frac{\partial y}{\partial x_i} = \frac{y_{\max} - y_{\min}}{x_{i,\max} - x_{i,\min}} \times \psi' \sum_{j=1}^{N_2} w_{ij} w_{j1} I_{jk}(1 - I_{jk}) \quad (15)$$

$$RMS_i = \sqrt{\frac{1}{S}\sum_{k=1}^{S}(d_{ik})^2} \quad (16)$$

where S = total number of model samples; k = 1, 2, …, 125; $y_{\max}$ = maximum output of network model; $y_{\min}$ = minimum output of network model; $x_{i,\max}$ = maximum value of x_i in the network model input; $x_{i,\min}$ = minimum value of x_i in network model input, and I = 1, 2, 3, 4, 5; ψ'= the derivative of the propagation function of the output layer (ψ(x) = x), ψ'=1; j = the number of hidden layer neurons (1, 2, …, 14); I_{jk} = the response of the j-th hidden layer neuron to the k-th model sample, I_{jk} (1-

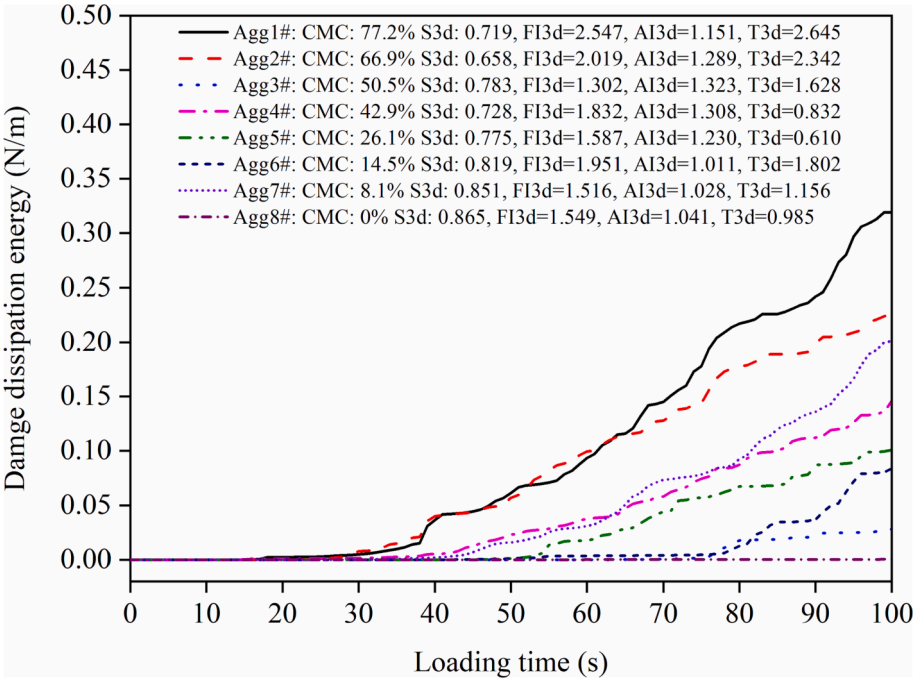

Fig. 5. The relationship between loading time and DDE of asphalt mortar-RCA interface.

$I_{jk}) = \psi'(I_{jk})$; w_{ij} = connection weight of i-th input parameter-j-th hidden neuron; w_{j1} = connection weight of j-th hidden neuron – output parameter.

5. Results and discussion

5.1. Adhesion damage behavior characteristics

The energy-based indicator DDE was proposed to characterize the damage evolution of asphalt mortar-RCA interface during uniaxial compression simulation. Once DDE > 0, it represents micro-crack initiation in the asphalt mortar–aggregate system [16]. As shown in Fig. 5, eight typical RCA particles were selected as examples to evaluate the interface damage behavior under load. It can be clearly observed that all interfacial DDEs of eight RCAs increased with loading time, indicating that the interface adhesion failure developed gradually due to loading. Moreover, the time of damage initiation showed a good relationship with the CMC parameter of RCA. CMC value growth led to an earlier damage initiation and a higher DDE value on the asphalt mortar-RCA interface under load. For example, the 1# RCA with the highest CMC value showed the earliest damage initiation (15 s) and the maximum DDE at the end of loading. The results illustrate that the CMC parameter of RCA exhibited a more noticeable influence on the interface adhesion than the other four parameters. A high CMC value could result in poor adhesion quality of asphalt mortar-RCA interface.

To expose the distribution characteristics of adhesion failure at the asphalt mortar-RCA interface, the RCA and corresponding interface elements in the numerical simulation were extracted, as listed in Fig. 6. The green particles represent RCAs without load, while the blue particles describe the interface damage state after 100 s load time. These 3D finite element models provide a simple visual understanding of the adhesion failure distribution at the interface. It can be found that when the RCA showed a higher CMC value and more complex morphology, the corresponding interface had more complete failure area (SDEG = 1), such as 1# RCA (CMC = 77.2 %). Compared to 1# RCA, the interface of 8# RCA appeared little complete failure area. The results indicate that the RCA with high CMC value, complex shape and surface leads to worse interface adhesion failure after damage initiation.

5.2. Adhesion damage prediction

As mentioned above, the preparation of ANN model and the analysis approach of prediction output were reported. Additionally, according to previous research results and trial calculation, we designated the related parameters in the GA-based BP ANN model as shown in Table 3. It is recommended that the crossover probability should show a high value, while the mutation probability is commonly low, about 0.5 %-1%. The maximum number of iterations is generally designated as 1000, and the value of learning rate is selected variously [35,36]. The population size (M) of GA and the number of neurons in the hidden layer (N_2) show significant influences on the feasibility of prediction output results [32]. So, Minimum MSE law was used to compare the accuracy of prediction results in the network model established by five M levels (20, 40, 60, 80, 100) and nine N_2 variables (4, 6, 8, 10, 12, 14, 16, 18, 20), respectively. In this case, it was possible to determine the most reasonable parameter in the network model.

It can be found from Fig. 7 that the M and N_2 parameters in the prediction model affect the accuracy of output results. Higher or lower N_2 parameters (e. g., M = 20, N_2 = 4 or 20) resulted in higher MSE of the prediction results. The different levels of the M parameter also allow the network model to output distinct prediction results. Generally, the MSE of different output results all meet the requirement of pre-defined (MSE $\leq$ 0.001), and the network model with 60 population and 14 hidden neurons showed the lowest MSE value. According to the minimum MSE law, the 5–14-1 (input layer-hidden layer-output layer) GA-based BP ANN model with a population size of 60 was undertaken to predict the adhesion behavior of asphalt mortar-RCA interface.

Table 3
The model parameters utilized in the GA-based BP ANN model.

Algorithm	Parameter	Levels
GA	Population size M	20, 40, 60, 80, 100
	Crossover probability p_c	0.6
	Mutation probability p_m	0.08
	Maximum number of generations G_{max}	200
BP	Number of hidden neurons N_2	4, 6, 8, 10, 12, 14, 16, 18, 20
	Learning efficiency η	0.1
	Maximum number of iterations T_{max}	1000

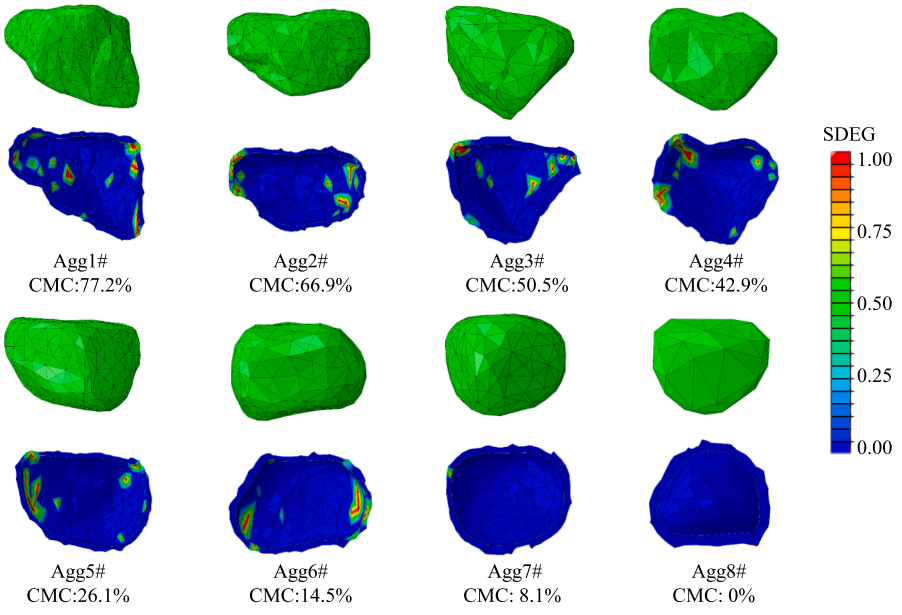

Fig. 6. Adhesion damage distribution for different asphalt mortar-RCA interface.

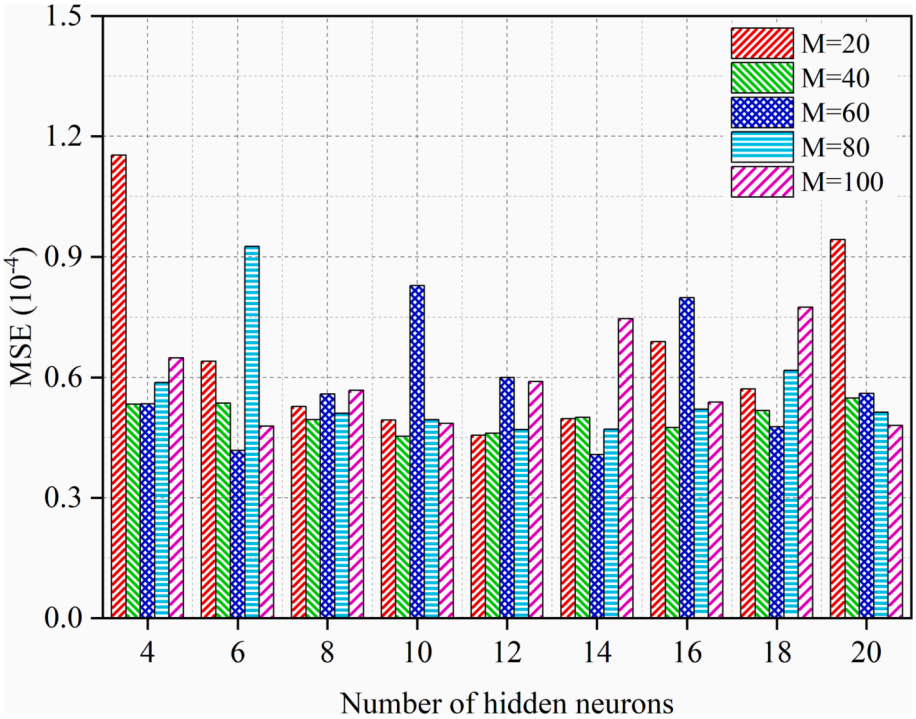

Fig. 7. The effect of M and N_2 parameters on network model performance.

Fig. 8(a) compares the uniaxial compression test results of 125 RCA particles by using finite element analysis and GA-based BP ANN model. The DDE values between different RCAs exhibited a significant variation range. It illustrates that the RCA features influence the interface adhesion of asphalt mortar-RCA system. In addition, it is noted that there is almost no difference between simulation test results and network model results. The deviation percentages between the predicted DDE value and tested DDE value of RCAs were all less than 5 %. It can also be verified by the linear relationship between FEM results and ANN prediction results, with an R^2 value of 0.98 and an MSE value of 3.52×10^{-4}. It indicates that the proposed GA-based BP ANN model in the current study can validly predict the adhesion damage of the asphalt mortar-RCA interface. It facilitates comprehensively evaluating the effect of RCA features on interface damage.

5.3. *Effect of RCA features on adhesive damage*

The above research results have confirmed the effect of RCA features on the adhesion damage of the asphalt mortar-RCA interface. A CSA method based on the prediction results of the network model was proposed to determine the relative contribution of various factors to interface adhesion. The RCA feature parameters include CMC, S_{3D}, FE_{3D}, AI_{3D}, ST_{3D}. And using the DDE parameter to quantify the interface adhesion damage.

As shown in Fig. 9(a), RCA's CMC parameter exhibited the most significant global relative contribution to interface adhesion, followed by FE_{3D} and S_{3D}, and ST_{3D} had the poorest effect on interface behavior. Hu et al. also reported similar results [16,17]. The RMS of CMC parameter was twice more than that of ST_{3D}, which indicates that the CMC parameter had the most significant effect on the interfacial adhesion quality. Compared to natural aggregate, higher porosity and lower modulus of cement mortar remaining degraded the mechanical property

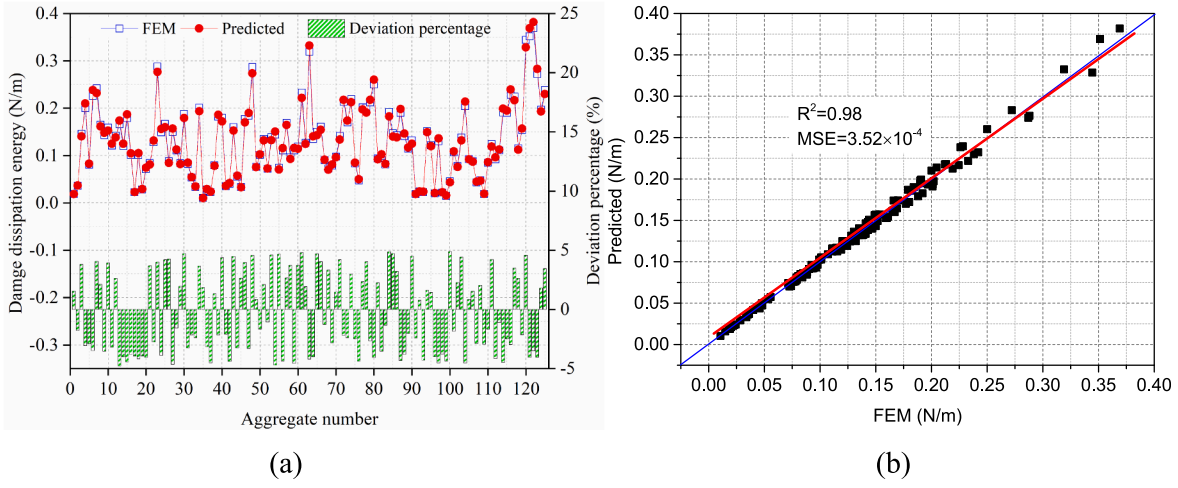

Fig. 8. DDE values of different asphalt mortar-RCA interface; (a) Comparison of FEM and ANN results; (b) linear relationship between FEM and ANN results.

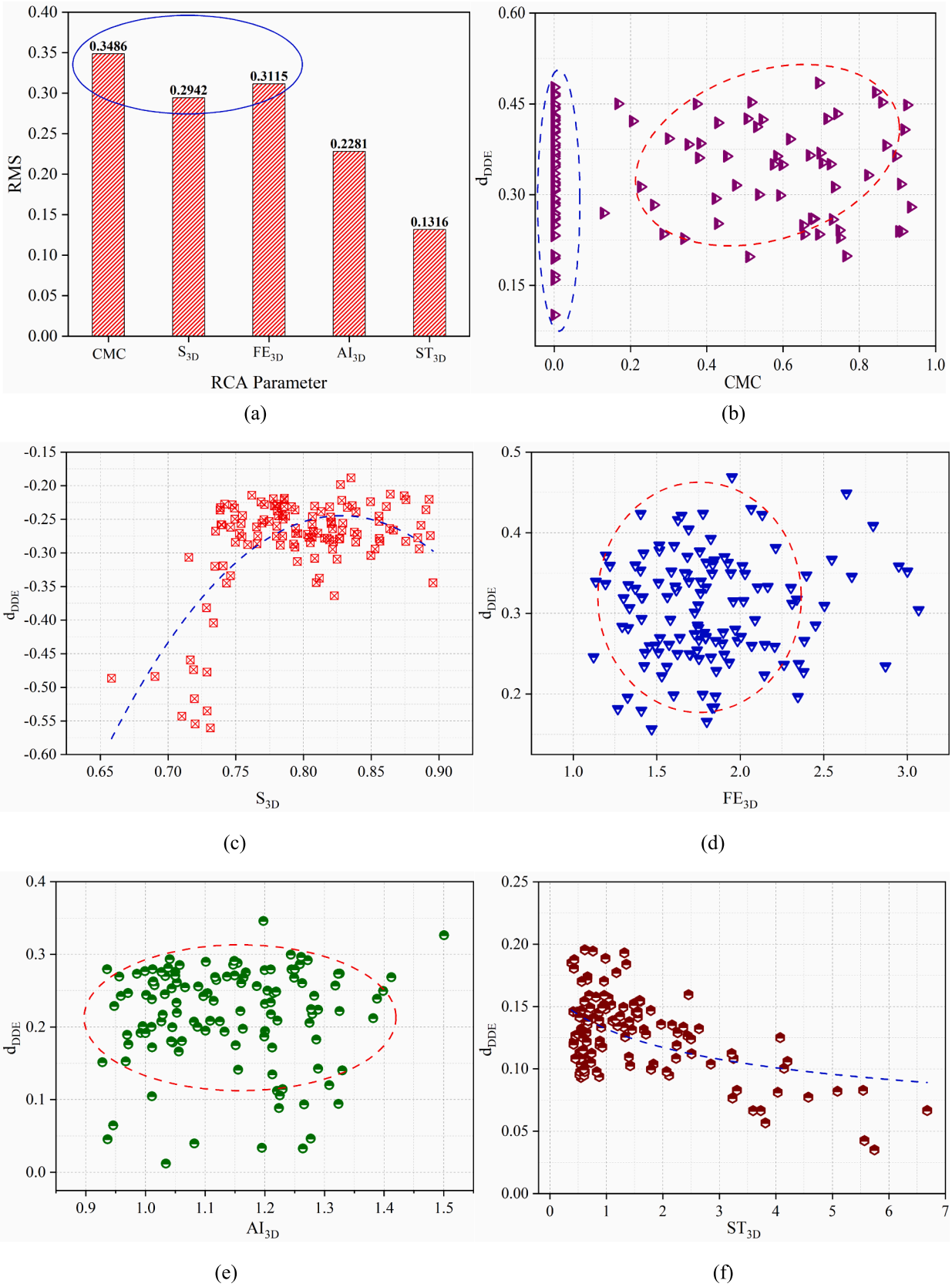

Fig. 9. Sensitivity analysis of the influence of RCA features on interfacial DDE; (a) RMS; (b) CMC; (c) S_{3D}; (d) FE_{3D}; (e) AI_{3D}; (f) ST_{3D}.

of the interface transition zone between asphalt mortar and RCA [17,42]. In addition, in Fig. 9(b), Fig. 9 (d), Fig. 9(e), Fig. 9(f), the local relative contribution showed a positive correlation ($d_{DDE} > 0$) with the corresponding RCA feature parameters. The results show that the interfacial DDE levels improved with the increase of CMC, FE_{3D}, AI_{3D}, and ST_{3D} values. It indicates that the asphalt mortar-RCA interface trended to adhesion failure. On the contrary, the S_{3D} had a negative local relative contribution to the DDE indicator ($d_{DDE} < 0$). This is due to the fact that RCA particle is more similar to a homogeneous sphere when the S_{3D} value increases. It facilitates relieving the stress concentration and interfacial adhesion damage between asphalt mortar and RCA particle [16,45]. It can also be observed that when the S_{3D} value increased from 0.65 to 0.75, the absolute value of relevant d_{DDE} showed a remarkable reduction. Therefore, using the RCA with the S_{3D} value greater than 0.75 may be beneficial to improve the adhesion quality of asphalt mortar-RCA interface.

6. Conclusions

This study observed the adhesion damage behavior of the asphalt mortar-RCA interface through the finite element simulation based on CZM. A GA-based BP artificial neural network was then utilized to predict the adhesion damage characteristics of 125 interfaces. According to the predicted results, a sensitivity analysis method was used to evaluate the effect of different RCA features on the interface adhesion quality. The following conclusions can be obtained.

(1) The RCA with high CMC, complicated shape and surface led to an earlier damage initiation time and complete adhesion failure on the interface. However, it is difficult to establish the quantified correlation between different RCA feature factors and interface adhesion by numerical simulation.
(2) The 5–14-1 GA-based BP ANN model designed in this study effectively predicted the interfacial DDE values after 100 s loading action. For the DDE results of different asphalt mortar-RCA, the correlation between numerical test and network prediction was fairly good, with an R^2 value of 0.98 and an MSE value of 3.52×10^{-4}.
(3) RCA's CMC, FE_{3D} and S_{3D} parameters exhibited significant global relative contribution to interface adhesion. And the CMC's corresponding RMS was more than twice that of ST_{3D} with the smallest global contribution.
(4) Increasing the values of CMC, FE_{3D}, AI_{3D}, and ST_{3D} parameters resulted in accelerating interface adhesion failure, while the S_{3D} parameter made a negative contribution. It is suggested that ensuring the S_{3D} value greater than 0.75 may facilitate the interface adhesion quality.

Overall, based on the results obtained from this study, it can be concluded that the CMC parameter has the most influence on the interface adhesion property. In future research, it is possible to further investigate the performance characteristics of cement mortar, thereby proposing the performance optimization technology of RCA. Moreover, a more refined mesh aggregate model (smaller mesh size) could be established by using a computer with better operational capability, which leads to a more accurate simulation result of interface adhesion damage. The technology of measuring the adhesion damage of each asphalt mortar-aggregate interface in an accurate asphalt mixture model should be proposed, resulting in obtaining more actual adhesion damage behavior of each asphalt mortar-aggregate interface.

CRediT authorship contribution statement

Haisheng Ren: Investigation, Resources, Writing – original draft. **Zhendong Qian:** Conceptualization, Methodology, Supervision. **Bin Lin:** Methodology. **Qibo Huang:** Conceptualization, Investigation, Resources. **Maurizio Crispino:** Supervision, Writing – review & editing. **Misagh Ketabdari:** Writing – review & editing.

Declaration of Competing Interest

The authors declare that they have no known competing financial interests or personal relationships that could have appeared to influence the work reported in this paper.

Data availability

Data will be made available on request.

Acknowledgment

The authors sincerely acknowledge the funding support from the Postgraduate Research & Practice Innovation Program of Jiangsu Province (KYCX21_0125) and the National Natural Science). The authors would like to thank the financial support to this research from the China Scholarship Council (CSC).

References

[1] T.O. Adewuyi, M. Otali, Evaluation of Causes of Construction Material Waste: Case of River State, Nigeria, Ethiop. J. Environ. Stud. Manag. 6(6) (2013) 746-753. https://doi.org/10.4314/ejesm.v6i6.5S.
[2] S.P. Raut, R.V. Ralegaonkar, S.A. Mandavgane, Development of sustainable construction material using industrial and agricultural solid waste: A review of waste-create bricks, Constr. Build. Mater. 25 (10) (2011) 4037–4042, https://doi.org/10.1016/j.conbuildmat.2011.04.038.
[3] N. Guo, Z. You, Y. Zhao, Y. Tan, A. Diab, Laboratory performance of warm mix asphalt containing recycled asphalt mixtures, Constr. Build. Mater. 64 (2014) 141–149, https://doi.org/10.1016/j.conbuildmat.2014.04.002.
[4] J. Mills-Beale, Z. You, The mechanical properties of asphalt mixtures with Recycled Concrete Aggregates, Constr. Build. Mater. 24 (3) (2010) 230–235, https://doi.org/10.1016/j.conbuildmat. 2009.08.046.
[5] M. Alamri, Q. Lu, C. Xin, Preliminary Evaluation of Hot Mix Asphalt Containing Reclaimed Epoxy Asphalt Materials, Sustainability 12 (9) (2020) 3531, https://doi.org/10.3390/su12093531.
[6] M.J. Chen, Y.D. Wong, Porous asphalt mixture with 100% recycled concrete aggregate, Road Mater. Pavement Des. 14 (4) (2013) 921–932, https://doi.org/10.1080/14680629.2013.837839.
[7] C. Maduabuchukwu Nwakaire, S. Poh Yap, C. Chuen Onn, C. Wah Yuen, H. Adebayo Ibrahim, Utilisation of recycled concrete aggregates for sustainable highway pavement applications; a review, Constr. Build. Mater. 235 (2020) 117444. https://doi.org/10.1016/j.conbuildmat. 2019.117444.
[8] M.S. de Juan, P.A. Gutiérrez, Study on the influence of attached mortar content on the properties of recycled concrete aggregate, Constr. Build. Mater. 23 (2) (2009) 872–877, https://doi.org/10.1016/j.conbuildmat.2008.04.012.
[9] C.H. Lee, J.C. Du, D.H. Shen, Evaluation of pre-coated recycled concrete aggregate for hot mix asphalt, Constr. Build. Mater. 28 (1) (2012) 66–71, https://doi.org/10.1016/j.conbuildmat. 2011.08.025.
[10] J. Thomas, N.N. Thaickavil, P.M. Wilson, Strength and durability of concrete containing recycled concrete aggregates, J. Build. Eng. 19 (2018) 349–365, https://doi.org/10.1016/j.jobe.2018.05.007.
[11] V.W.Y. Tam, C.M. Tam, K.N. Le, Removal of cement mortar remains from recycled aggregate using pre-soaking approaches, Resour. Conserv. Recycl. 50 (1) (2007) 82–101, https://doi.org/10.1016/j.resconrec.2006.05.012.
[12] A.R. Pasandín, I. Pérez, B. Gómez-Meijide, N. Pérez-Barge, The Effect of Hydrated Lime on the Bond Between Asphalt and Recycled Concrete Aggregates, Pet. Sci. Technol. 33 (10) (2015) 1141–1148, https://doi.org/10.1080/10916466.2014.984076.
[13] F.M. Nejad, A.R. Azarhoosh, G.H. Hamedi, The effects of using recycled concrete on fatigue behavior of hot mix asphalt, J. Civ. Eng. Manag. 19(sup1) (2013) S61-S68. https://doi.org/10.3846/13923730.2013.801892.
[14] B. Huang, X. Shu, G. Li, L. Chen, Analytical Modeling of Three-Layered HMA Mixtures, Int. J. Geomech. 7 (2) (2007) 140–148, https://doi.org/10.1061/(ASCE)1532-3641(2007)7:2(140).
[15] X.Y. Zhu, Z.X. Yang, X.M. Guo, W.Q. Chen, Modulus prediction of asphalt concrete with imperfect bonding between aggregate–asphalt mastic, Compos. B Eng. 42 (6) (2011) 1404–1411, https://doi.org/10.1016/j.compositesb.2011.05.023.
[16] J. Hu, Z. Qian, The prediction of adhesive failure between aggregates and asphalt mastic based on aggregate features, Constr. Build. Mater. 183 (2018) 22-31. https://doi.org/10.1016/j.conbuildmat.2018.06.145.
[17] Q. Huang, Z. Qian, J. Hu, D. Zheng, L. Chen, M. Zhang, J. Yu, Investigation on the properties of aggregate-mastic interfacial transition zones (ITZs) in asphalt mixture containing recycled concrete aggregate, Constr. Build. Mater. 269 (2021), 121257, https://doi.org/10.1016/j.conbuildmat.2020.121257.

[18] P. Kuusela, M. Pour-Ghaz, R. Pini, A. Voss, A. Seppänen, Imaging of reactive transport in fractured cement-based materials with X-ray CT, Cem. Concr. Compos. 124 (2021), 104211, https://doi.org/10.1016/j.cemconcomp.2021.104211.
[19] F. San José Martínez, F.J. Muñoz Ortega, F.J. Caniego Monreal, A.N. Kravchenko, W. Wang, Soil aggregate geometry: Measurements and morphology, Geoderma 237–238 237-238 (2015) 36–48.
[20] B. Cantero, M. Bravo, J. de Brito, I.F. Sáez del Bosque, C. Medina, Mechanical behaviour of structural concrete with ground recycled concrete cement and mixed recycled aggregate, J. Cleaner Prod. 275 (2020), 122913, https://doi.org/10.1016/j.jclepro.2020.122913.
[21] W.R.V. Brian D. Aho, Samuel H. Carpenter, Effect of Flat and Elongated Coarse Aggregate on Field Compaction of Hot-Mix Asphalt, Transport. Res Rec. J. Transport. Res. Board. 1761(1) (2001) 26-31. https://doi.org/https://doi.org/10.3141/1761-04.
[22] X. Yang, S. Chen, Z. You, 3D Voxel-Based Approach to Quantify Aggregate Angularity and Surface Texture, J. Mater. Civ. Eng. 29 (7) (2017) 04017031, https://doi.org/10.1061/(asce)mt.1943-5533.0001872.
[23] M.A. Maroof, A. Mahboubi, A. Noorzad, Y. Safi, A new approach to particle shape classification of granular materials, Transp. Geotech. 22 (2020) 100296. https://doi.org/10.1016/j.trgeo.2019.100296.
[24] Y.R. Kim, F.A.C. de Freitas, J.S. Jung, Y. Sim, Characterization of bitumen fracture using tensile tests incorporated with viscoelastic cohesive zone model, Constr. Build. Mater. 88 (2015) 1–9, https://doi.org/10.1016/j.conbuildmat.2015.04.002.
[25] Y. Zhang, X. Luo, R. Luo, R.L. Lytton, Crack initiation in asphalt mixtures under external compressive loads, Constr. Build. Mater. 72 (2014) 94–103, https://doi.org/10.1016/j.conbuildmat.2014.09.009.
[26] L. Chang, N. Kaijian, Simulation of asphalt concrete cracking using Cohesive Zone Model, Constr. Build. Mater. 38 (2013) 1097–1106, https://doi.org/10.1016/j.conbuildmat.2012. 09.063.
[27] S.M. Motevalizadeh, H. Rooholamini, Cohesive zone modeling of EAF slag-included asphalt mixtures in fracture modes I and II, Theor. Appl. Fract. Mech. 112 (2021), 102918, https://doi.org/10.1016/j.tafmec.2021.102918.
[28] E. Amoosoltani, A. Ameli, F. Jabari, S. Asadi, Employing a hybrid GA-ANN method for simulating fracture toughness of RCC mixture containing waste materials, Constr. Build. Mater. 272 (2021), 121928, https://doi.org/10.1016/j.conbuildmat.2020.121928.
[29] G.M. Mabrouk, O.S. Elbagalati, S. Dessouky, L. Fuentes, L.F. Walubita, Using ANN modeling for pavement layer moduli backcalculation as a function of traffic speed deflections, Constr. Build. Mater. 315 (2022), https://doi.org/10.1016/j.conbuildmat.2021.125736.
[30] M. Gevrey, I. Dimopoulos, S. Lek, Review and comparison of methods to study the contribution of variables in artificial neural network models, Ecol. Model. 160 (3) (2003) 249–264, https://doi.org/10.1016/s0304-3800(02)00257-0.
[31] X. Li, L. Shu, L. Liu, D. Yin, J. Wen, Sensitivity analysis of groundwater level in Jinci Spring Basin (China) based on artificial neural network modeling, Hydrogeol. J. 20 (4) (2012) 727–738, https://doi.org/10.1007/s10040-012-0843-5.
[32] D. Zheng, Z.D. Qian, Y. Liu, C.B. Liu, Prediction and sensitivity analysis of long-term skid resistance of epoxy asphalt mixture based on GA-BP neural network, Constr. Build. Mater. 158 (2018) 614–623, https://doi.org/10.1016/j.conbuildmat.2017.10.056.
[33] ASTM C 78, Standard Test Method for Flexural Strength of Concrete (Using Simple Beam with Third-Point Loading, American Society for Testing and Materials, 2021.
[34] AASHTO TP 114, Standard method of test for determining the interlayer shear strength (ISS) of Asphalt pavement layers, American Association of State Highway and Transportation Officials, 2015.
[35] T. Baklacioglu, O. Turan, H. Aydin, Dynamic modeling of exergy efficiency of turboprop engine components using hybrid genetic algorithm-artificial neural networks, Energy 86 (2015) 709–721, https://doi.org/10.1016/j.energy.2015.04.025.
[36] H.H. Örkcü, H. Bal, Comparing performances of backpropagation and genetic algorithms in the data classification, Expert Syst. Appl. 38 (4) (2011) 3703–3709, https://doi.org/10.1016/j.eswa.2010.09.028.
[37] L.T. Mo, M. Huurman, S.P. Wu, A.A.A. Molenaar, Bitumen–stone adhesive zone damage model for the meso-mechanical mixture design of ravelling resistant porous asphalt concrete, Int. J. Fatigue 33 (11) (2011) 1490–1503, https://doi.org/10.1016/j.ijfatigue.2011.06.003.
[38] Y. Lu, L. Wang, Nano-mechanics modelling of deformation and failure behaviours at asphalt–aggregate interfaces, Int. J. Pavement Eng. 12 (4) (2011) 311–323, https://doi.org/10.1080/10298436.2011.575136.
[39] H. Wang, E. Lin, G. Xu, Molecular dynamics simulation of asphalt-aggregate interface adhesion strength with moisture effect, Int. J. Pavement Eng. 18 (5) (2015) 414–423, https://doi.org/10.1080/10298436.2015.1095297.
[40] D. Kuang, B. Zhang, Y. Jiao, J. Fang, H. Chen, L. Wang, Impact of particle morphology on aggregate-asphalt interface behavior, Constr. Build. Mater. 132 (2017) 142–149, https://doi.org/10.1016/j.conbuildmat.2016.11.132.
[41] M. Horgnies, E. Darque-Ceretti, H. Fezai, E. Felder, Influence of the interfacial composition on the adhesion between aggregates and bitumen: Investigations by EDX, XPS and peel tests, Int. J. Adhes. Adhes. 31 (4) (2011) 238–247, https://doi.org/10.1016/j.ijadhadh.2011.01.005.
[42] J. Hu, P. Liu, Q. Huang, Z. Qian, S. Luo, Research on interfacial zone failure of asphalt mixture mixed with recycled aggregates, Constr. Build. Mater. 319 (2022), 126113, https://doi.org/10.1016/j.conbuildmat.2021.126113.
[43] H. Ban, P. Karki, Y.-R. Kim, Nanoindentation Test Integrated with Numerical Simulation to Characterize Mechanical Properties of Rock Materials, J. Test. Eval. 42 (3) (2014), https://doi.org/10.1520/jte20130035.
[44] P. Karki, Y.-R. Kim, D.N. Little, Dynamic Modulus Prediction of Asphalt Concrete Mixtures through Computational Micromechanics, Transport, Res Rec. J. Transport. Res. Board. 2507 (1) (2019) 1–9, https://doi.org/10.3141/2507-01.
[45] J. Hu, Z. Qian, Q. Huang, P. Liu, Investigation on high-temperature stability of recycled aggregate asphalt mixture based on microstructural characteristics, Constr. Build. Mater. 341 (2022), 127909, https://doi.org/10.1016/j.conbuildmat.2022.127909.